Journal of Catalysis 422 (2023) 12–23

Contents lists available at ScienceDirect

Journal of Catalysis

journal homepage: www.elsevier.com/locate/jcat

ReO_x as a Brønsted acidic modifier in glycerol hydrodeoxygenation: Computational insight into the balance between acid and metal catalysis

Ville Korpelin [a,1], Gokarneswar Sahoo [a,b,1], Rasmus Ikonen [a], Karoliina Honkala [a,*]

[a] Department of Chemistry, Nanoscience Center, University of Jyväskylä, P.O. Box 35, 40014, Jyväskylä, Finland
[b] Department of Chemistry, National Institute of Technology Rourkela, Rourkela 769008, Odisha, India

ARTICLE INFO

Article history:
Received 17 November 2022
Revised 21 March 2023
Accepted 22 March 2023
Available online 05 April 2023

Keywords:
Hydrogenolysis
Hydrodeoxygenation
Glycerol
Density functional theory
Heterogeneous catalysis
Rhodium
Rhenium

ABSTRACT

A computational study for the competitive conversion of glycerol to 1,2-propanediol and 1,3-propanediol is presented, considering a two-step sequence of dehydration followed by hydrogenation. The elementary steps for dehydration, i.e., breaking of C–H followed by C–OH or vice versa, were studied computationally both on the Rh metal surface and the acid-modified ReOH–Rh surface in order to understand the role of the acid promoter. While the acid modifier can catalyze the C–OH cleavage, the activation energy for the C–H cleavage was found to be considerably smaller on both pure and acid-doped Rh(111) surfaces, and breaking the secondary C–H bond is kinetically favored over breaking the terminal C–H bond. This is in complete agreement with experimental protocols favoring the formation of 1,2-propanediol. Another potential feedstock, glycidol, was studied for the epoxide ring opening to yield 1,2-propanediol and 1,3-propanediol, and the reaction was found to be metal-catalyzed even in the presence of acid.

1. Introduction

Glycerol is one of the smallest polyols and is by-produced in enormous amounts in biodiesel production. Moreover, glycerol, which can be produced from carbohydrates, has been identified as a building block molecule for value-added chemical production [1]. All of this makes glycerol an attractive low-cost feedstock. Although there are several routes for converting glycerol to other chemicals,[1–7] one of the most attractive transformations is the selective catalytic hydrodeoxygenation, which comprises the removal of hydroxyl groups by addition of hydrogen. The desirable catalytic route converts glycerol to 1,2-propanediol (1,2-PDO) and 1,3-propanediol (1,3-PDO), but also propanol, ethanol, methanol, etc. (Scheme 1) can be formed. Among these deoxygenated intermediates, the straight-chain diol 1,3-PDO finds numerous industrial applications including, e.g., composites, adhesives and co-polymers (Scheme 1) [8]. Currently, 1,3-PDO is produced industrially employing petroleum-based feedstocks and using either acrolein (Degussa/Dupont process) or ethylene oxide (Shell process) as starting material [2]. The desired selective hydrogenolysis of biomass-derived glycerol into 1,3-PDO is not satisfactory,[9–13] since glycerol conversion is low and selectivity is hampered by the formation of less valuable 1,2-PDO and other degraded products such as acrolein [14]. In particular, propanediol selectivity favors 1,2-PDO, which is the thermodynamically preferred species over kinetically controlled 1,3-PDO formation [3].

Glycerol conversion to 1,3-PDO has been explored on various supported transition metal catalysts including, e.g, Cu-, Ru-, Pt- and Rh-based catalysts [15–19]. Experimental studies highlight that a significant amount of 1,3-PDO is only formed in the presence of a co-catalyst, which typically is the oxide of group 6 or 7 metal [10]. In the literature, e.g., ReO_x-modified Ru, Rh and Ir catalysts and WO_x-modified Rh and Pt have been reported to catalyze glycerol transformation to 1,3-PDO [6,9,15,20–24]. In a combined experimental and computational study,[11] the selective hydrogenolysis of polyols and cyclic ethers over a ReOH–Rh catalyst was reported to occur due to the stability of a secondary oxocarbenium ion formed during the first dehydration step [11]. However, while the cyclic ethers showed good selectivity towards the cleavage of the ether bond to produce the most stable carbocation, the diol selectivity of glycerol was quite poor.

Since the first mechanistic interpretation of glycerol conversion to 1,2-PDO,[25] several other mechanistic pathways have been proposed (Scheme 2), depending on whether the system is acidic, basic or metallic [26]. Three types of reaction mechanisms are generally accepted:[5] (a) dehydration–hydrogenation; b) dehydrogenation-dehydration–hydrogenation; (c) direct hydrogenolysis [10,22]. As the dehydration–hydrogenation pathway is typically

* Corresponding author.
E-mail address: karoliina.honkala@jyu.fi (K. Honkala).
[1] These authors contributed equally.

https://doi.org/10.1016/j.jcat.2023.03.032
0021-9517/

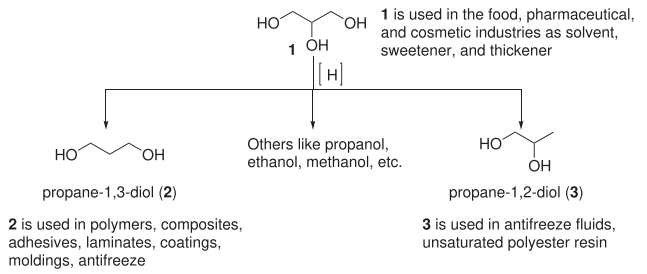

scheme 1. Transformation of glycerol to diols [8,5].

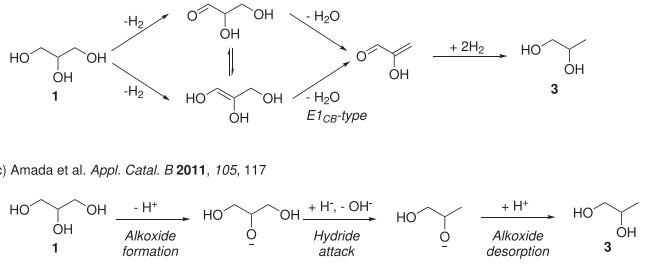

scheme 2. Reported mechanisms of glycerol dehydration towards 1,2-PDO and/or 1,3-PDO. (a) dehydration–hydrogenation; (b) dehydrogenation-dehydration–hydrogenation; c) direct hydrogenolysis.

proposed for acidic systems,[5,26] it is chosen as the focus of this study to explore the Brønsted acidic role of the ReO_x modifier. We note, however, that the direct hydrogenolysis mechanism has also been proposed for oxophilic modifiers [3,6].

Computationally, the C–H, C–C, and C–O bond breaking steps for glycerol have been addressed on the (111) surface of different transition metals employing density functional theory (DFT) calculations, elucidating both thermodynamic and kinetic trends for the decomposition of glycerol into a variety of fragments [19,27]. Other DFT studies have concentrated on the selected reaction pathways for glycerol conversion on transition metal surfaces [17,18,28,29]. In Ref. [17], both thermodynamic and kinetic factors for 1,2-PDO and lactic acid selectivity on Rh(111) were investigated. These calculations found that the main product from the initial dehydration should be prop-1-ene-1,3-diol, which converts to 1,3-PDO, but that glyceraldehyde formation via dehydrogenation is kinetically preferred and leads to the experimentally observed 1,2-PDO product by a further dehydration and hydrogenation pathway. Despite the large number of studies, the atomic level understanding of 1,2-PDO and 1,3-PDO selectivity has remained elusive.

In the present work, we have employed DFT calculations to analyze the hydrogenolysis of glycerol, focusing in particular on the critical dehydration step, which controls selectivity towards either 1,2-PDO or 1,3-PDO. Two different catalysts were studied: bare Rh modelled with a Rh(111) surface, and ReO_x-modified Rh modelled with ReOH–Rh(111). Both the adsorption energies of all concerned intermediates and the corresponding activation energies were determined on bare Rh(111) and in the presence of a ReOH co-catalyst to elucidate the role of the acid for selectivity. Finally, we have addressed the glycerol-derived epoxide, glycidol, as a potential reactant and explored the metal- and acid-catalyzed ring opening chemistry.

2. Methods

The density functional theory calculations were performed with the GPAW code,[30,31] which implements the projector augmented wave method (PAW)[32] in a real space grid. The ASE interface was used to set up the calculations [33]. The Kohn–Sham equations were solved self-consistently using the PBE GGA[34] (generalized gradient approximation) functional to describe exchange and correlation effects. The van der Waals interactions were described by the Tkatchenko–Scheffler correction[35] as implemented in ASE/GPAW, with the parameters for Re and Rh taken from Ref. [36]. A four-layer thick slab was used to model a bare Rh(111) surface with an optimized lattice constant of 3.857 Å and a (3×3) unit cell. The acid-modified Rh(111) was modelled by replacing one Rh atom from the surface layer with the ReOH group. The $(2 \times 2 \times 1)$ Monkhorst–Pack k-point sampling was used throughout the work. The atomic structures were relaxed until residual forces were below 0.05 eV/Å with one bottom Rh layer frozen to the bulk positions. The adsorption energies were calculated as follows:

$$\Delta E_{ads} = E_{ads/surface} - E_{surface} - E_{ads(gas)}, \quad (1)$$

where the energies of a clean surface $E_{surface}$ and the adsorbate in a vacuum $E_{ads(gas)}$ are subtracted from the energy of the system, where the adsorbate is on the surface $E_{ads/surface}$. The reaction energies for glycerol dehydration were computed from

$$\Delta E_{react} = E_{int/surface} + E_{frag/surface} - E_{surface} - E_{C_3H_8O_3(gas)}, \quad (2)$$

where $E_{int/surface}$ is the total energy of the adsorbed intermediate, $E_{frag/surface}$ is the total energy of the adsorbed fragments cleaved from the intermediate (H, OH or H_2O), and the last two terms are the total energies of a clean surface and glycerol in the gas phase. The adsorbed fragments are taken to be at infinite separation from the intermediate, with H and OH combining to form H_2O when possible.

The transition states were located employing the climbing image nudged elastic band method[37–39] or a constrained search, where the interatomic distance of a breaking bond is fixed to several values and the remaining degrees of freedom are relaxed. The constrained search was found to perform well in cases of simple H transfer to the surface, while the more complicated surface reactions involving OH groups were better handled with the NEB approach. The transition states were verified via harmonic frequency calculation. One imaginary frequency was obtained for each transition state, and the visualization of the vibration mode showed bond stretching along a reaction coordinate. The activation barriers were calculated as follows:

$$E_{act} = E_{TS} - E_{ads/surface}, \quad (3)$$

where E_{act} is an activation barrier and E_{TS} and $E_{ads/surface}$ are the total energies of the transition state and precursor moieties, respectively.

3. Results and discussion

3.1. Adsorption of glycerol and its dehydrated products on Rh(111)

First, we address the adsorption geometries and thermodynamics of glycerol and its dehydration products on Rh(111) (Scheme 3). The most stable geometries are presented in Figs. 1 and 2, while Fig. 3 shows the corresponding adsorption energies.

Previous DFT studies [17–19,27] show that glycerol presents various adsorption modes on the Rh(111) surface, and our structure search was largely based on these previously reported conformers; in total, 12 different glycerol adsorption geometries were simulated. To evaluate the effect of the adsorption geometry, we chose to consider both a syn-syn and an anti-anti glycerol conformer for further analysis. The most stable geometries for each type are displayed in Fig. 1. Both structures bind to the surface through a terminal OH group, with a Rh–O bond length of 2.3 Å. The syn-syn conformer features two weak intramolecular hydrogen bonds between vicinal OH groups (bond lengths 2.49 and

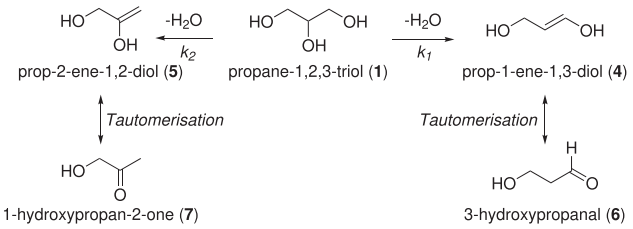

scheme 3. Dehydration of glycerol (**1**) to possible intermediates. This first dehydration step determines the product selectivity toward 1,2- or 1,3-PDO.

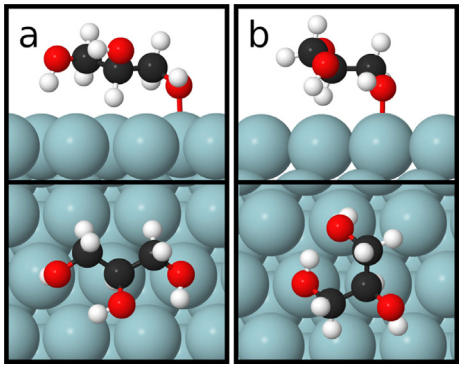

Fig. 1. Two glycerol conformations on Rh(111); (a) syn-syn conformation and (b) anti-anti conformation. The side-view pictures are oriented to have a better view of intramolecular interactions in the glycerol molecule.

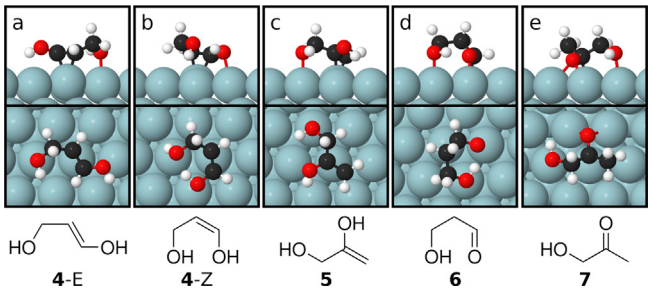

Fig. 2. The most strongly binding conformations of dehydrated intermediates of glycerol on a Rh(111) surface.

2.21 Å), while the anti-anti conformer features one strong hydrogen bond (1.79 Å) between the terminal OH groups. The syn-syn geometry differs from the one previously reported for Rh(111) [18], which we ascribe to the van der Waals interaction included in the present work favoring a more flat-lying geometry. Indeed, a closely matching structure was found especially favorable on Pt (111) when the vdW correction was included [40]. Our anti-anti geometry also differs slightly from the most commonly reported structure,[17,18,27] in which the O atom of the secondary hydroxyl also interacts with the surface, but matches the one described in Ref. [19]. We find the energetic difference between the two to be small at 0.04 eV, with enhanced vdW interactions in our geometry likely compensating for the lost Rh–O binding. The syn-syn and anti-anti geometries in Fig. 1 are thermodynamically equivalent with each other, with an adsorption energy difference of only 0.01 eV.

The most stable geometries of the keto and enol forms of the dehydrogenation products are presented in Fig. 2. Tautomers **5** and **7** can be hydrogenated to form 1,2-PDO, while tautomers **4** and **6** convert to 1,3-PDO. The enol intermediates (**4** & **5**) bind more strongly than their corresponding carbonyl counterparts (**6** & **7**

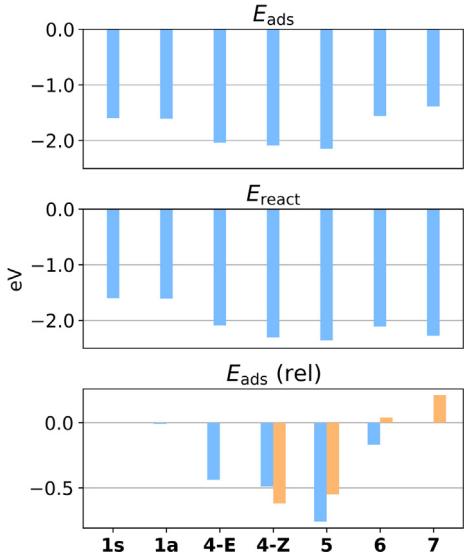

Fig. 3. Adsorption energies (E_{ads}) and reaction energies (E_{react}) of glycerol and its dehydrated intermediates on Rh(111). The energies are computed according to Eqs. (1) and (2). The relative ("rel") energies are calculated relative to syn-syn glycerol in order to facilitate comparison between our vdW-corrected energies (blue) and the PW91 literature values (orange) [18]. **1s**/**1a** refers to the syn-syn/anti-anti glycerol conformation. The data is provided in numerical form in Table S1 of the supplementary material.

respectively), which partly highlights the higher stability of the keto species in the gas phase. Interestingly, the binding of enol species **4** and **5** is more exothermic than the binding of glycerol, whereas for keto intermediates it is vice versa. Intermediate **4** has two structural isomers, **4**-E and **4**-Z; previous studies report the Z isomer as a possible result from the dehydration of glycerol [17]. The Z isomer is about 0.2 eV more stable than the E isomer due to an internal hydrogen bond, which is not possible for the E isomer. Both **4**-E and **4**-Z species bind to the surface via the C–C double bond and one terminal oxygen on the atop position with a near-planar molecular structure. Intermediate **5** is the most stable enol species, and it also binds to the surface via the C–C double bond and a terminal hydroxyl. The average C–Rh distance for the double bond C is 2.17–2.19 Å for each enol intermediate, while the Rh–O bond lengths are 2.29–2.37 Å. The C–C double bond lengths are 1.42–1.43 Å, stretched by 0.08–0.09 Å from the corresponding lengths in the gas phase. All the enol species thus adsorb in a very similar manner.

The carbonyl isomers **6** and **7** both bind to the surface via their carbonyl and hydroxyl groups. While the double bonds of the most stable enol intermediates adsorb atop Rh atoms, the carbonyl pi bonds instead prefer bridging sites. In aldehyde **6**, the carbonyl oxygen is near a Rh top site, while in aldehyde **7**, it lies closer to a bridge site. The carbonyl bond lengths are 1.375 and 1.386 Å, respectively, both about 0.16 Å longer than in the gas phase. These binding geometries agree with an earlier study on glycerol dehydration products on Rh(111) [18]. Compared to that work, we find a smaller relative adsorption energy for aldehyde **6** (Fig. 3). This is probably related to the vdW correction we have applied here: as aldehyde **6** binds through its terminal groups, the methylene moieties are fairly distant from the surface, leading to a smaller vdW stabilization.

Some structures were also optimized without including the van der Waals correction, making it possible to study its effects on the energies and geometries. Broadly, the vdW correction makes the adsorption energies more exothermic by 1.0 to 1.4 eV, indicating a considerable van der Waals contribution to the surface–molecule

interaction. A similar stabilizing effect of ∼1 eV was found for glycerol adsorption on various Pt surfaces using the D3 correction [40]. Overall, the vdW correction tends to more strongly stabilize geometries that are in close proximity to the surface. While the direct molecule–surface bond lengths are only slightly affected, the more distant parts of the molecules are brought closer to the surface.

Fig. 3 also presents the reaction energies of dehydration products **4**, **5**, **6**, and **7**, and allows us to consider the thermodynamic preference of different dehydration pathways. The reaction energies of enols **4** and **5** demonstrate that enol **5**, which leads to 1,2-PDO, is thermodynamically slightly more stable than enol **4**. Likewise, aldehyde **7** is more stable than aldehyde **6** by 0.17 eV, meaning that the 1,2-PDO route is thermodynamically favored by both keto and enol forms. This would be in agreement with experimental observations that the 1,2-PDO pathway is favored over the 1,3-PDO one [11,20,41,42].

3.2. Kinetic preference of C–H cleavage over C–OH cleavage

Having confirmed the thermodynamic favorability of dehydration toward 1,2-PDO, we now consider the kinetics of the process. The dehydration of glycerol to enols **4** and **5** is crucial for determining the selectivity between 1,3- and 1,2-PDO, and so we focus on this part of the reaction network. Enols **4** and **5** respectively yield 1,3-PDO and 1,2-PDO by hydrogenation, possibly after tautomerizing to their respective carbonyl counterparts **6** and **7**. The tautomerization and hydrogenation steps are excluded from the present study, as their effect on the selectivity is expected to be minor. On bare Rh(111), we have mainly considered a sequential elimination process, where the C–H and C–O bond cleavages occur consecutively via a strongly surface-bound intermediate (Scheme 4). To evaluate the kinetic preference of the dehydration process, we determined transition states and activation energies for each elementary bond breaking step in Scheme 4. The alternative possibilities of alkoxide formation and concerted dehydration will be discussed later.

Within our scheme, the initial step can be either a C–O cleavage (Scheme 4, path a) or a C–H cleavage (Scheme 4, path b). The labels a_{11} and a_{12} correspond to C–O cleavage at the secondary carbon followed by C–H cleavage at a primary carbon, while b_{11} and b_{12} represent the same steps in the opposite order; both processes result in intermediate **4**. The labels a_{21}, a_{22}, b_{21} and b_{22} follow the same logic, except the cleaved bonds are primary C–O and secondary C–H, producing intermediate **5**. Previous DFT calculations for dehydration of ethanol on Rh(111) predict that C–H bond cleavage takes place before the C–O cleavage [43–46]. Similar results have been obtained for ethylene glycol on Pt(111),[47] suggesting that this is a typical feature of alcohols on late transition metals. Nevertheless, we address both a and b pathways to verify the trend and to quantify the effect of the acid modifier introduced later. Fig. 4 displays the potential energy surface for glycerol transformation to enols **4** and **5** together with the transition state geometries. The energies are presented relative to gas-phase glycerol and bare Rh, and include the adsorbed H/OH/H_2O fragments that are cleaved during the reaction. The fragments are assumed to diffuse far away from the molecules after each elementary step.

The first C–O cleavage of glycerol along paths a_{11} and a_{21} demonstrates high activation energies, 1.90 eV and 1.83 eV, compared to the initial C–H activation energies of 0.84 eV and 0.57 eV (paths b_{11} and b_{21}). As expected, the initial C–O cleavage is highly unfavorable, and the first step should thus be a C–H cleavage. Our values are generally consistent with previous results for ethanol on Rh(111), for which initial C–O cleavage barriers of 1.76–2.21 eV have been reported [43–46]. For the corresponding glycerol reaction on Rh(111), the only literature value we found

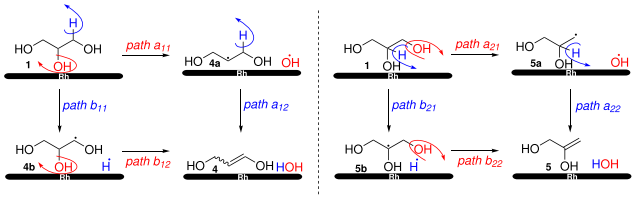

scheme 4. Dehydration of glycerol (**1**) to intermediates **4** and **5**. The notion path X_{mn} represents X = a for C–OH cleavage followed by C–H cleavage and b for the reverse process; $m = 1$ for glycerol to prop-1-ene-1,3-diol, 2 for glycerol to prop-2-ene-1,2-diol; $n = 1$ for the first elementary process involving conversion of glycerol to the radical species, 2 for the second elementary process involving the conversion of radical species to the dehydrated enol intermediate. C–OH cleavage steps are colored red, while steps related to C–H cleavages are colored blue. (For interpretation of the references to colour in this figure legend, the reader is referred to the web version of this article.)

is 1.29 eV for the a_{11} step,[19] which is 0.61 eV lower than our result. This surprisingly low barrier was determined by a scaling relation based approach, with relations derived from the reactions of dehydrogenated intermediates on Pt(111); the scaling model thus might not be able to describe the behavior of an intact glycerol molecule on Rh(111) due to the different electronic structures of these molecules. The initial C–H cleavage barriers for ethanol and glycerol on Rh(111) are typically in the 0.5–0.8 eV range, [17,19,27,43,46,48] also consistent with our results, though values of over 1.0 eV have also been reported [43–45,49]. Some of these higher barriers may be related to the chosen initial geometry disfavoring a particular bond scission, as pointed out in Ref. [27].

The effect of the initial geometry is also notable for glycerol. In contrast to a previous study of glycerol on Rh(111), where terminal C–H cleavage was found kinetically 0.06 eV more favorable than central C–H cleavage,[17] our results show that central C–H cleavage is favored by 0.27 eV. This difference can be attributed to the initial glycerol geometry: the central C–H bond of the anti-anti glycerol considered in the present work points directly toward the surface, and thus it can easily be cleaved. On the other hand, the terminal C–H cleavage is sterically hindered on this conformer, as the adjacent groups prevent the reacting terminal C atom from easily reaching a stabilizing surface Rh atom. The terminal C–H cleavage step b_{11} was therefore initiated from a more amenable geometry, also resulting in a facile reaction ($E_{act} = 0.62$ eV). However, this alternative conformer is thermodynamically less stable by 0.22 eV than the anti-anti one, and thus less likely to exist on the surface; therefore, the central C–H cleavage originating from the anti-anti conformer is expected to be the dominant initial step. The observed difference in C–H cleavage barriers favors path b_2 leading to enol **5**, and partially explains the experimental preference of glycerol hydrogenolysis toward 1,2-PDO over 1,3-PDO [11,20,41,42].

After each initial step, a different surface intermediate is formed. The relative reaction energies (see Eq. 2) of the intermediates depend on the reaction path: while the **4a** and **4b** intermediates are thermodynamically almost equivalent, **5b** has a more exothermic reaction energy than **5a**. The order of the reaction energies (**5b** < **4a** ≈ **4b** < **5a**) can be explained by considering the stabilities of the adsorbed intermediate species. First, Rh(111) binds H more strongly than OH, favoring the **4b** and **5b** species, though this effect is partially compensated by the higher inherent stability of the dehydroxylated species. Second, the secondary radicals are more stable than the primary radicals, favoring **4a** and **5b**. Taken together, these factors reflect the reaction energy order: intermediate **5b** is favored by both of these factors, **5a** is favored by neither, and **4a** and **4b** are each favored by one.

In the second step on the reaction pathway, the **a** and **b** intermediates undergo C–H and C–O cleavages, respectively. The sec-

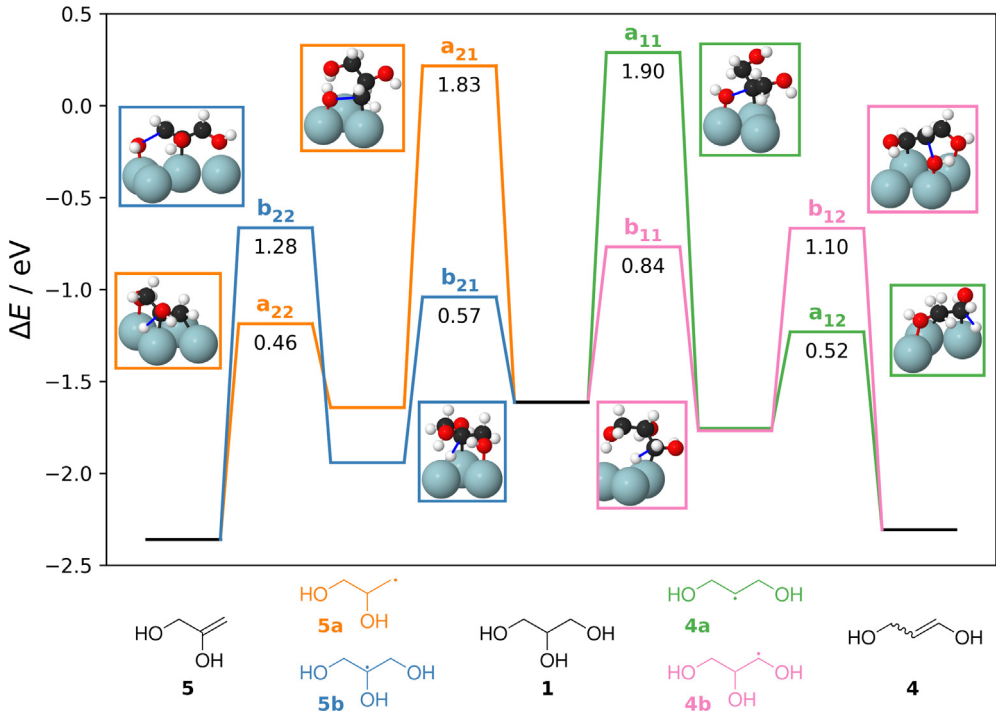

Fig. 4. Potential energy surface for dehydration of glycerol on a Rh(111) surface. Green curve: conversion of glycerol to **4** through path a; pink curve: glycerol to **4** through path b; orange curve: glycerol to **5** through path a; blue curve: glycerol to **5** through path b. All energies are given respect to glycerol in gas-phase. The activation energies given in the figure are reported with respect to the most stable adsorption structure of the reacting species. We note that TS-b_{11} was found on an alternative syn-syn conformation of glycerol, as discussed in the text. (For interpretation of the references to colour in this figure legend, the reader is referred to the web version of this article.)

ond C–O cleavage steps b_{12} and b_{22} have activation energies of 1.10 and 1.28 eV, which are 0.80 and 0.55 eV lower than those of the corresponding initial C–O cleavages a_{11} and a_{21}. The second C–O cleavages are more exothermic by ca. 0.4 eV and feature late transition states, which is expected to lower the barrier according to the Brønsted-Evans-Polanyi principle: the a_{11} and a_{21} transition states resemble the relatively unstable intermediates, while the b_{12} and b_{22} transition states resemble the stable dehydration products. The second dehydroxylation barriers are both slightly higher than those reported in the literature (Table 1), possibly due to a strong vdW stabilization of the **4b** and **5b** intermediates relative to glycerol. The geometries and relative stabilities of the two transition states are in good agreement with prior results [17]. The second C–H cleavage steps a_{12} and a_{22} also have slightly lower barriers than the corresponding initial steps b_{11} and b_{21}. The difference in reaction energies between the first and second steps is again about 0.3 eV, but the effect on the barriers is less pronounced. In general, the barrier for breaking a given C–H or C–O bond is lower for the surface intermediates than for the intact glycerol molecule, and the difference is larger for C–O cleavage.

The transition state geometries shown in Fig. 4 exhibit multiple common features. Upon C–O cleavage, the OH group ends up atop a Rh atom (Rh–O distance 2.1 Å at TS), as this site is the most readily accessible from the reactant adsorption geometries. At each transition state, the C–O bond has elongated from 1.4 to ca. 2.1 Å, while the reacting C atom is 2.3–2.4 Å from the nearest Rh atom. In the C–H transition states, the position of the leaving H atom varies between top, bridge and in-between sites. The shortest Rh–H distance is about 1.6 Å in each case, while the C–H bond lengths range from 1.5 to 1.7 Å. All the C–O and C–H cleavages can therefore be characterized as having late transition states. There is no correlation between individual TS bond lengths and activation energies, indicating the activation energy depends on multiple interactions between the surface, reactant and leaving group. In general, the C–O bond breaking steps have higher barriers than the C–H bond breaking steps, which arises from the greater molecular distortion required to expel the OH group and the comparatively weak Rh–OH interaction at the TS geometry.

Table 1
Activation energies for the elementary steps computed in the present study and existing literature values. The literature values for transition states b_{11}, b_{12}, b_{22} are reported on the Pt(111) surface. a = Ref. [19] for Rh(111), b = Ref. [19] for Pt(111), c = Ref. [17] for Rh(111).

TS	E_{act}/eV	literature value
TS-a_{11}	1.90	1.29[a]
TS-a_{12}	0.74	nd
TS-a_{21}	1.83	nd
TS-a_{22}	0.53	nd
TS-b_{11}	0.84	0.84[b], 0.77[c]
TS-b_{12}	1.10	1.21[b], 0.94[c]
TS-b_{21}	0.57	0.76[a], 0.83[c]
TS-b_{22}	1.28	1.41[b], 1.20[c]

Comparing the enol **4** (1,3-PDO) and enol **5** (1,2-PDO) reaction pathways, the potential energy surfaces are quite similar. The thermodynamics and kinetics of the initial steps favor the b_2 pathway towards 1,2-PDO, although the second C–O cleavage step b_{22} is slower than the corresponding b_{12} step on the b_1 pathway. In Ref. [17], both barriers along the b_1 path were found lower than the corresponding b_2 barriers on Rh(111) (Table 1), indicating that this elimination mechanism should clearly favor 1,3-PDO formation. As discussed before, the adsorption geometries considered in our work favor secondary C–H cleavage and thus 1,2-PDO formation, highlighting the kinetic effect of the reactant conformer. A real catalytic system comprises an ensemble of reactant conformations, each with their own features favoring some steps over others.

To round out the discussion, we address some reactions outside of our sequential dehydration scheme, starting with concerted

dehydration. The a_{21} transition state was identified as a promising template for such a reaction, as there is an H atom very close to the surface on the middle carbon. Indeed, this H atom can be removed simultaneously with the OH group to directly form enol **5**, but the barrier for the concerted reaction is still high at 1.81 eV. The dehydration reactions are therefore expected to proceed via consecutive C–H and C–O cleavage steps, as discussed before.

Finally, while we have primarily focused on the C–H and C–O cleavages, there is the additional possibility of O–H cleavage, i.e., alkoxide formation. This has been reported as viable for glycerol on Rh(111), with a barrier of about 0.70 eV and an athermic or mildly exothermic reaction energy,[17,27] indicating that it could compete with the initial C–H scission. We also considered the alkoxide thermodynamics, and our results agree with the literature: primary alkoxide formation is essentially thermoneutral (−0.04 eV), while secondary alkoxide formation is somewhat exothermic (−0.31 eV). In a comprehensive treatment of the reaction network, alkoxide formation could thus be a relevant factor, and modifier-bound alkoxides have been proposed as active intermediates [20,50]. However, our main interest is to analyze the effect of the acid modifier, and this can be accomplished in the framework of C–H and C–O scissions.

3.3. Adsorption of glycerol and its dehydrated products on ReOH–Rh (111)

To explore the impact of an acidic co-catalyst, we introduced a ReOH moiety onto the Rh(111) surface such that Re replaces one surface Rh atom, as shown in Fig. 5. The resulting structure can be considered a Rh–Re single atom alloy[51] with an adsorbed hydroxyl group. A similar model has been computationally studied for the hydrogenolysis of cyclic ethers, and the ReOH modifier embedded in Rh was found more acidic than either a hydroxyl group on pure Rh or a monomeric ReOH modifier adsorbed on top of the surface [11,52]. Herein, we investigated how such a co-catalyst modifies the thermodynamic and kinetic properties of glycerol dehydration, assuming a molecular ratio of 1:1 for the organic moiety and the ReOH modifier. While some molecules could favorably interact with two ReOH moieties due to the periodicity of the model, all adsorption geometries (Figs. 5 and 6) were chosen such that only one direct molecule–ReOH interaction is present in order to facilitate energy comparisons.

Fig. 5 displays the syn-syn and anti-anti glycerol conformations on ReOH–Rh(111), showing that the addition of ReOH does not qualitatively change the glycerol geometries. The added hydrogen bonding with ReOH stabilizes the syn-syn and anti-anti conformations by −0.05 and −0.13 eV, respectively (Fig. 7), whereas each dehydrated intermediate can form a hydrogen bond with ReOH in two different ways: via a carbinol OH group, or via an enol OH/-carbonyl O group. Both possibilities were considered for each molecule. The most stable adsorption geometries are shown in Fig. 6, and the corresponding adsorption energies are shown in Fig. 7. While some intermediates could form two simultaneous hydrogen bonds with the ReOH modifier, this was only found favorable when molecule **5** forms a hydrogen bond via its enol group (Fig. 6h). Even then, the corresponding geometry with a single carbinol H-bond (Fig. 6c) is more stable, showing that such dual hydrogen bonding is not the most favorable binding motif for the dehydrated intermediates.

Comparing the hydrogen bonding via carbinol and enol or carbonyl groups, we observe that bonding via the carbinol OH is more favorable for all enol species (**4**-E, **4**-Z and **5**). This behavior arises from the geometric properties of the enols. The molecules are unable to form a strong enol-OH–ReOH hydrogen bond while maintaining the C–C double bond in its most favorable position

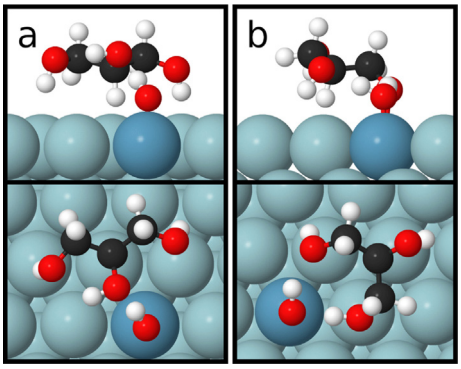

Fig. 5. Adsorption of (a) syn-syn and (b) anti-anti conformations of glycerol on ReOH-Rh(111). The color code is as in Fig. 1, except the Re atom is colored blue. (For interpretation of the references to colour in this figure legend, the reader is referred to the web version of this article.)

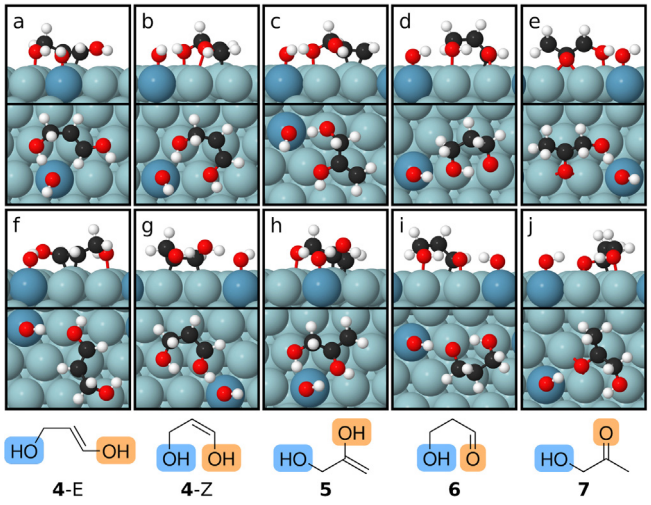

Fig. 6. Adsorption conformations of different dehydrated intermediates derived from glycerol on ReOH-Rh(111). Subfigures a–e represent the H-bond between carbinol OH group (shaded blue) and ReOH, subfigures f–j represent the H-bond between enol-OH/carbonyl-O group (shaded orange) and ReOH. (For interpretation of the references to colour in this figure legend, the reader is referred to the web version of this article.)

atop a Rh atom. This results in either a weak hydrogen bond (Fig. 6f) or an unfavorable C–C-Rh interaction (Figs. 6g and 6h). On the other hand, the carbinol OH group is separated from the C–C double bonds by a methylene group, allowing the double bond and hydroxyl to simultaneously reach stable configurations (Figs. 6a–c). The addition of acid stabilizes enol **4**-Z slightly less than the other enols, as its existing intramolecular hydrogen bond is disturbed by the added ReOH bonding.

For the aldehydes, the situation is different: aldehyde **6** favors H bonding via its carbonyl O, while aldehyde **7** exhibits the opposite behavior. There are two geometric reasons for this. The hydroxyl group of aldehyde **6** can participate in intramolecular hydrogen bonding, while the hydroxyl of adsorbed aldehyde **7** cannot. This allows ReOH hydrogen bonding to stabilize the OH group more effectively in aldehyde **7** than in aldehyde **6**. In addition, the carbonyl group of aldehyde **6** lies atop a Rh atom, making it more available for H bonding than the bridging carbonyl of aldehyde **7**. In general, the stability differences between the carbinol and enol/carbonyl H-bonded structures appear to be largely governed by geometric details rather than inherent differences in hydrogen bonding strengths.

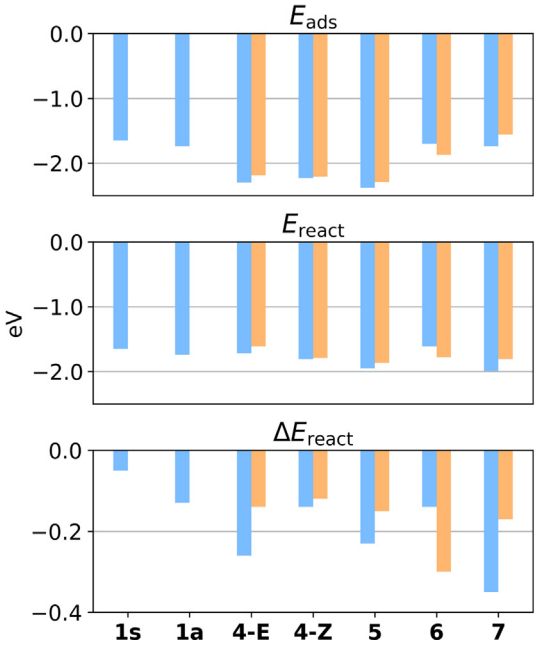

Fig. 7. Adsorption and reaction energies on ReOH–Rh(111). The blue/orange bars represent species with hydrogen bonds via carbinol/enol OH groups. **1s**/**1a** refers to the syn-syn/anti-anti glycerol conformation. ΔE_{react} is the difference between reaction energies on ReOH–Rh(111) and bare Rh(111), i.e., the stabilization due to molecule–ReOH interaction. The data is provided in numerical form in Table S2 of the supplementary material.

Considering the most stable structure for each dehydrated species, the trend observed on bare Rh(111) is retained, as intermediates **5** and **7** leading to 1,2-PDO are more stable than intermediates **4** and **6** leading to 1,3-PDO. The difference becomes slightly more pronounced on ReOH–Rh(111), as the 1,2-PDO intermediates feature at most weak intramolecular hydrogen bonding on Rh(111). This allows them to interact with the ReOH modifier without affecting any existing stable hydrogen bonds, slightly stabilizing **5** and **7** relative to the intramolecularly hydrogen bonded species **4**-Z and **6**.

3.4. Influence of acid on the dehydration kinetics of glycerol

Having established that the thermodynamics of glycerol dehydration still favor 1,2-PDO on ReOH–Rh(111), we now turn to the kinetics. The Brønsted acidic ReOH modifier is expected to stabilize the C–O cleavage transition states by protonating the reacting hydroxyl into a water molecule, thereby forming a better leaving group. While the ReOH modifier can also affect the C–H cleavage barriers by modifying the reactant adsorption properties, we found this mildly unfavorable, in agreement with previous studies on the effect of intermolecular hydrogen bonding on the reactions of alcohols on Rh(111) [27,28]. We have therefore assumed that the C–H cleavages take place over bare Rh(111), and the ReOH modifier is considered for C–O bond breaking.

The computed potential energy surface for glycerol dehydration on ReOH–Rh(111) is shown in Fig. 8, while Fig. 9 provides the corresponding energy values for both Rh and ReOH–Rh. The results highlight the effectiveness of the acid catalyst, as the initial C–O cleavage barriers are lowered by 0.76 (a_{11}) and 0.46 eV (a_{21}). The removal of the secondary OH thus becomes substantially more favorable, but still has a higher barrier than the corresponding initial C–H cleavage. The effect of the acid on the second C–O cleavage steps, b_{12} and b_{22}, is much smaller, being only −0.20 and −0.07 eV. In both cases, the elimination of secondary hydroxyl becomes easier than that of the primary one, increasing the kinetic favorability toward 1,3-PDO over 1,2-PDO. While the b_{21} dehydrogenation leading to enol **5** is still the fastest initial step, the barrier for the following b_{22} step is now higher than any of the barriers on the way to enol **4**, indicating that the processes are more competitive. These observations are in line with experimental results: when ReO_x is introduced to a Rh catalyst, activity and 1,3-PDO selectivity are increased, but the selectivity of 1,3-PDO (∼ 25 %) remains lower than that of 1,2-PDO (30–40 %) [11,20,53].

Like the C–O cleavage steps on bare Rh(111), the corresponding acid catalyzed reactions feature late transition states. At the TS, the water molecule has already been formed and almost separated from the carbon skeleton, as evidenced by the short water O–H bond lengths (1.0–1.1 Å) and the long C–O distances (2.0–2.2 Å). In three of the studied transition states (a_{11}, a_{21} and b_{12}), the water molecule is only interacting with the surface via hydrogen bonding to the deprotonated ReO. In the b_{22} TS, the water molecule is instead formed on the surface, as the reacting hydroxyl group lies atop a Rh atom. The strong H_2O–Rh interaction is expected to stabilize the TS considerably, but the effect is likely counterbalanced by the unfavorable non-planar geometry of the nascent C–C double bond.

In experimental studies comparing the effects of metal oxide modifiers on glycerol hydrogenolysis on Rh and Ir, 1,3-PDO selectivity follows the order Ir–ReO_x > Ir–WO_x > Ir–MoO_x > Rh–ReO_x > Rh–WO_x > Rh–MoO_x [20,21]. The computationally predicted deprotonation energies of the corresponding monomeric modifiers on Rh and Ir follow exactly the opposite trend,[52] suggesting that higher acidity favors 1,3-PDO formation. In addition, ReO_x acid sites with higher Re–O coordination have been predicted to feature more acidic protons than terminal ReOH groups [50,52]. These results suggest that the monomeric modifier studied in the present work may underestimate the catalyst acidity and 1,3-PDO selectivity. On the other hand, as the experimental selectivity on Rh–ReO_x is also comparatively poor, monomeric ReOH seems sufficiently acidic to model the dehydration reaction. Apart from the acid strength, the structure of the modifier also determines the active site geometry; while embedded (“alloy”) and adsorbed (“cluster”) ReO_x modifiers have comparable acidities,[52] their catalytic properties may differ due to geometric reasons.

The acid activation of glycerol hydroxyl groups has previously been simulated in a $Re_3O_6H_3$/Ir(111) system, in which the modifier was adsorbed rather than embedded [50]. The protonation–dehydration of the secondary hydroxyl in a physisorbed glycerol molecule, corresponding to step a_{11} in Fig. 8, was found to have a high barrier of 2.04 eV. In fact, this barrier was 0.21 eV higher than that of direct C–OH cleavage on bare Ir(111). In our simulations on ReOH–Rh(111), the a_{11} protonation–dehydration barrier is instead 0.76 eV *lower* than the corresponding C–OH cleavage on bare Rh (111). This substantial difference could be related to the different oxide geometries chosen for the simulations. As the $Re_3O_6H_3$ cluster was placed on top of the Ir surface, the glycerol molecule physisorbed onto the cluster lies relatively far from the metal component. This likely hinders the ability of the metal to stabilize the reacting C atom at the TS, leading to a high activation energy. As our ReOH modifier is instead embedded into the Rh(111) surface, the metallic component can easily stabilize the acid-catalyzed TS geometry in a bifunctional manner. On $Re_3O_6H_3$/Ir (111), the reaction was determined to proceed through easily formed cluster alkoxides, for which the protonation–dehydration barriers of the primary and secondary hydroxyls are 1.74 and 1.28 eV, respectively. These barriers are higher than those we found on ReOH–Rh(111), but exhibit a greater discrimination between primary and secondary hydroxyls. This is in qualitative agreement with the experimental observation that ReO_x–Ir is less active but more selective than ReO_{x-Rh} [21].

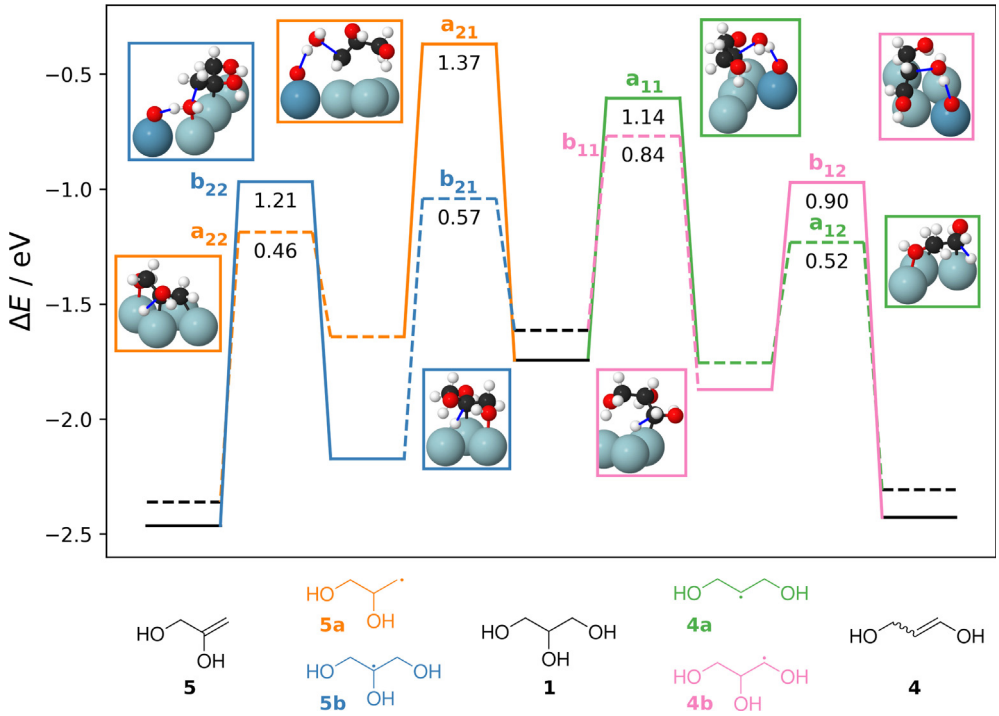

Fig. 8. Potential energy surface for dehydration of glycerol on ReOH–Rh(111). Energies are given with respect to glycerol in gas-phase. The solid and dashed lines represents the parts simulated on ReOH–Rh(111) and bare Rh(111), respectively (see text). Green curve: conversion of glycerol to **4** through path a; pink curve: glycerol to **4** through path b; orange curve: glycerol to **5** through path a; blue curve: glycerol to **5** through path b.

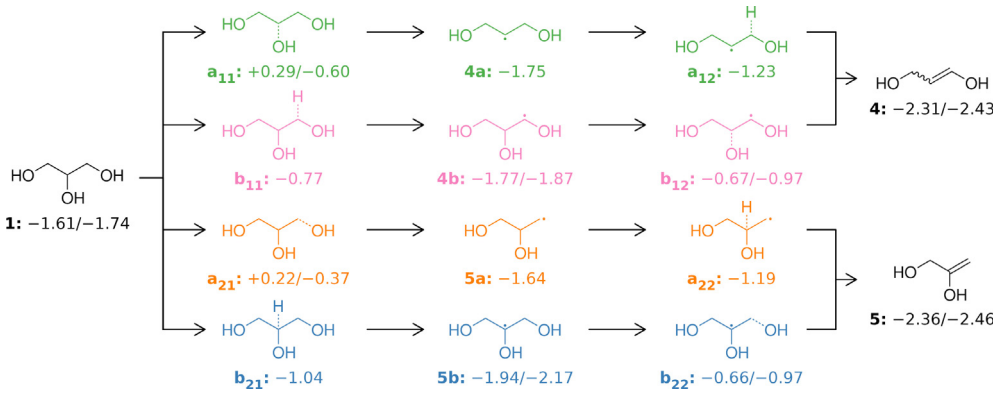

Fig. 9. Complete reaction mechanism with reaction energies in eV for each adsorbed species and transition state on Rh (before slash) and ReOH–Rh(111) (after slash). The species with only one number were only considered on Rh(111). The bonds that are being cleaved in the TS structures are shown in dashed lines.

3.5. Glycidol: reductive cleavage of the epoxide ring

While Re–Rh catalysts are not highly selective in glycerol dehydration, they exhibit good selectivity in various ring-opening reactions [11,13,54–56]. This raises the interesting possibility of modifying the substrate instead of the catalyst, as glycerol can be converted into a cyclic ether, glycidol,[57,58] whose possible roles in glycerol valorization have been recently reviewed [58]. Propanediol synthesis from glycidol has been experimentally studied on acid-modified Ni- and Cu-based catalysts,[59,60] carbon- and alumina-supported metals,[61–63] and various Co-based catalysts [63]. Rh/Al_2O_3 and Rh/C were found to produce very little 1,3-PDO, while 1,2-PDO was a major product [62]. On the acid-modified Ni/Cu catalysts, most of the studied configurations also favor 1,2-PDO over 1,3-PDO, but a 1,3-PDO/1,2-PDO ratio of 1.24 was obtained over an optimized Ni–Re catalyst [60]. Among the modifiers studied (Mo, V, W and Re), Re was found the most selective toward 1,3-PDO. It is thus interesting to see whether the ReOH modifier on Rh can also steer the selectivity toward 1,3-PDO, and to this end, we carried out simulations of the initial ring-opening part of the reaction (Scheme 5).

The most stable glycidol conformations on Rh(111) and ReOH–Rh(111) are shown in Fig. 10. On Rh(111), both oxygen atoms bind on top of Rh atoms with respective Rh–O bond lengths of 2.33 and 2.47 Å for the epoxide and hydroxyl groups. Even though the groups are on top of adjacent Rh atoms, there is no intramolecular hydrogen bonding. The glycidol geometry is somewhat different from the one previously computed on Pd(111), which featured an agostic O–H–Pd interaction instead of a direct hydroxyl-O–Pd bond [64]. The difference can be attributed to the higher oxophilicity of Rh, with the vdW correction also possibly playing a role. On ReOH–Rh(111), the conformation is similar as on Rh(111), featuring a strong hydroxyl–ReOH hydrogen bond (1.625 Å) and a weak ReOH–epoxide-O interaction (2.535 Å). The adsorption energies

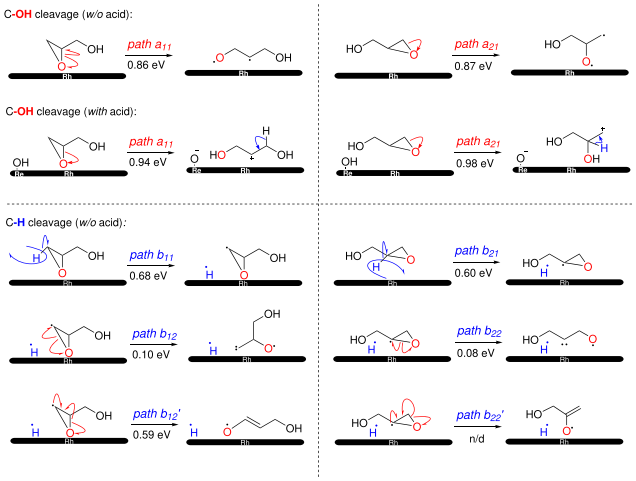

scheme 5. Ring opening of glycidol. The notion path X_{mn} represents X = a for C–O cleavage followed by C–H cleavage and b for the reverse process; $m = 1$ for glycerol to prop-1-ene-1,3-diol, 2 for glycerol to prop-2-ene-1,2-diol; $n = 1$ for the first elementary process involving conversion of glycidol to the radical species. C–OH cleavage steps are colored red, while steps related to C–H cleavages are colored blue. (For interpretation of the references to colour in this figure legend, the reader is referred to the web version of this article.)

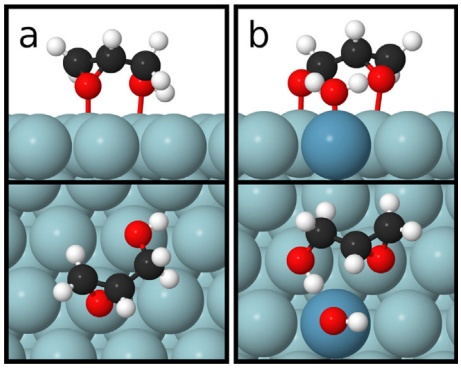

Fig. 10. Adsorption conformations of glycidol on (a) Rh(111) and (b) ReOH–Rh (111).

on Rh(111) and ReOH–Rh(111) are −1.28 eV and −1.50 eV, so the stabilization by ReOH interaction (−0.22 eV) is of similar magnitude for glycidol as for the dehydrated intermediates discussed before (Fig. 7).

To quantify the effect of the acid modifier on the ring opening, the C–O cleavage of glycidol was simulated on both Rh(111) and ReOH–Rh(111). As before, the C–H cleavages were assumed to take place on bare Rh(111). The resulting potential energy diagram is presented in Fig. 11, with the corresponding energy values shown in Fig. 12. The direct ring opening of glycidol is found to have a barrier of ca. 0.9 eV regardless of which C–O bond is cleaved. Surprisingly, the ReOH modifier has almost no effect on the barriers, indicating it is not sufficiently acidic to catalyze the reaction (Scheme 5). The slightly higher barrier for the acid-catalyzed reactions is due to a weakened hydroxyl–ReOH hydrogen bond at the discovered transition states. As discussed above, the monomeric oxide model may underestimate the acidity of the catalyst, and a more acidic species might be necessary to activate the reaction. An alternative possibility is that the reaction is initiated by an interfacial hydride attack instead of protonation [13,59].

On the other hand, similar computational models have been found to acid-catalyze the ring opening of tetrahydrofurfuryl alcohol (THFA), which can be considered a glycidol analogue with a 5-membered ring [11,52]. To analyze the differences in reactivity between the two molecules, we computed their gas-phase protonation energies, which have been noted as useful activity descriptors for Brønsted acid catalyzed reactions [65]. According to our results, gas-phase protonation of the ether oxygen is 0.86 eV more endothermic for glycidol than for THFA, indicating that the glycidol oxygen is more difficult to protonate (i.e., less basic). Indeed, glycidol is not protonated at the ring-opening TS, and only accepts the proton as the reaction proceeds further. This is in contrast to the reported THFA transition state, in which proton transfer has already occurred [11]. In addition to being more difficult to protonate, we note that glycidol has a higher ring strain than THFA, making it more unstable to begin with and possibly diminishing the effect of the acid.

The barriers for the C–H cleavage steps b_{11} and b_{21} are also close to each other, with b_{21} being both kinetically and thermodynamically favored. This is again in contrast to previous results for the larger THFA ring, for which activation at the less substituted ring carbon is preferred for steric reasons [11,66]. Steric effects could be less important for the smaller glycidol ring, making both C–H cleavages almost equally facile and causing the higher stability of the secondary radical formed by path b_{21} to play a larger role in the selectivity.

After the C–H cleavage, the ring opening can occur in two different ways: from the surface-bound dehydrogenated carbon atom (Scheme 5, steps b_{12} and b_{22}) or from the other ring carbon (b_{12}' and b_{22}'). The first mechanism has been proposed for THFA, [11,66] while the second one relies on the ability of the reactant to form a double bond between the ring carbons and is thus likely not feasible for larger rings. Both options were simulated, and the b_{12} and b_{22} mechanisms reported for larger rings were also found the most likely for glycidol, having barriers of only ∼0.1 eV. A transition state was also located for the alternative b_{12}' path, but the barrier is comparatively high at 0.68 eV. The difference is likely geometrical: the b_{12}' ring opening requires the molecule to undergo considerable reorientation, while the b_{12} and b_{22} mechanisms simply stretch open a surface-bound C–O bond.

In contrast with experimental results, our simulations predict that glycidol preferentially forms 1,3-PDO over 1,2-PDO on a Rh catalyst. This could be a consequence of the chosen mechanistic model; instead of the routes considered here, the ring-opening might instead be initiated by a hydride attack, which has been proposed to be selective for 1,2-PDO on glycidol and other similar rings [13,59]. Alternatively, the hydrogenation steps after ring-opening could be relevant. While the surface-adjacent ring opening has a very low barrier, so does the reverse reaction; however, we note that the path b ring-opening products can very exothermically donate another H atom to the bare Rh(111) surface, resulting in a highly dehydrogenated species that may be difficult to hydrogenate into a propanediol. The situation may well be different under realistic hydrogenolysis conditions, and H coverage has been reported to affect selectivity in, e.g., the reactions of furfural on Pd (111) [67].

4. Conclusions

The thermodynamics and kinetics of glycerol dehydration on acid-modified Rh have been simulated using DFT with van der Waals corrections. The present mechanistic study indicates that the dehydration of glycerol in heterogeneous medium over the Rh surface follows a path (path b) where the C–OH cleavage is preceded by a C–H cleavage from an adjacent C atom. The experimentally observed preference toward 1,2-PDO is related to a highly favorable secondary C–H cleavage.

The poor selectivity of glycerol hydrogenolysis on ReOH–Rh catalysts has been addressed computationally. In a Brønsted acid cat-

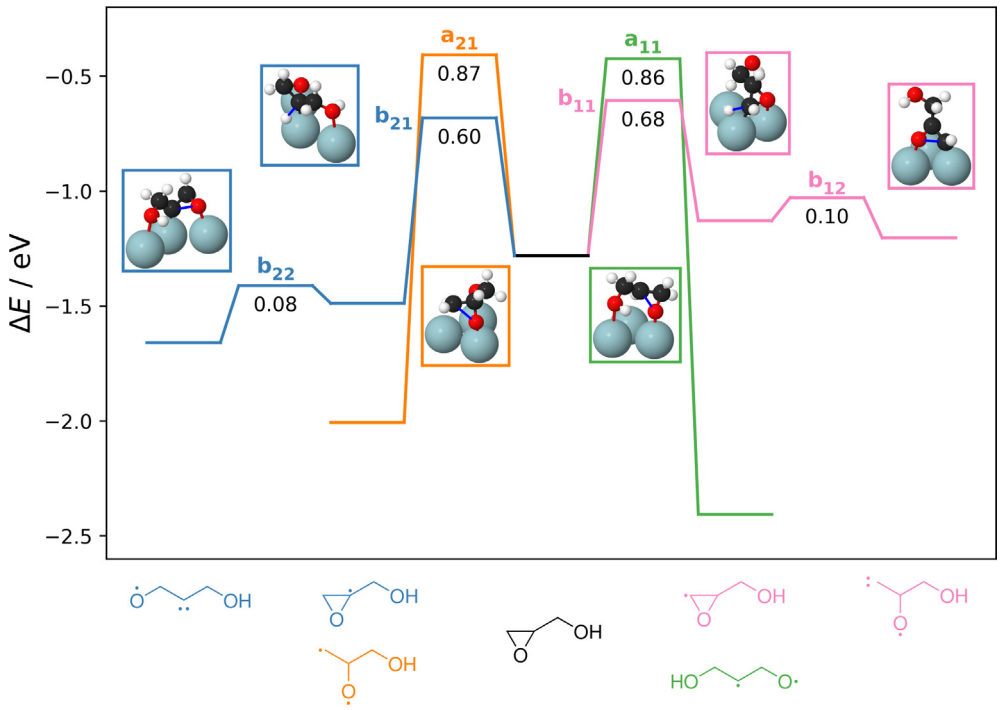

Fig. 11. Comparison of elementary steps for ring-opening of glycidol on Rh(111). Energies are given with respect to gas-phase glycidol.

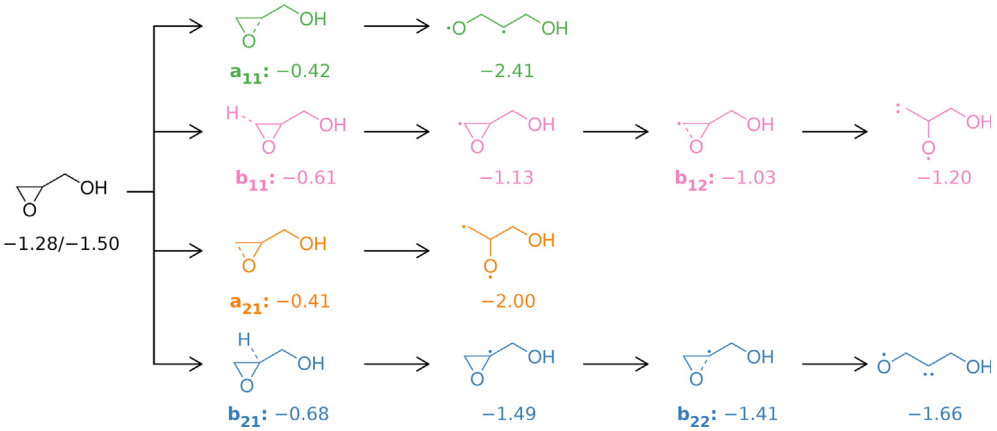

Fig. 12. Glycidol ring-opening mechanisms with reaction energies in eV for each adsorbed species and transition state on Rh (before slash) and ReOH–Rh(111) (after slash). The species with only one number were only considered on Rh(111). The bonds that are being cleaved in the TS structures are shown in dashed lines.

alyzed reaction, the selectivity is often determined by carbocation intermediate stabilities, favoring secondary C–OH cleavage in the case of glycerol. However, although the ReOH modifier considerably facilitates the initial C–O cleavage, its barrier remains higher than that of the C–H cleavage catalyzed by free Rh. The reaction can therefore be initiated by a dehydrogenation step, lowering the impact of carbocation stabilities. Stronger acids with lower H binding energies could cause the secondary C–O cleavage to overtake the C–H cleavages, which may explain the much better experimental 1,3-PDO selectivity reported for, e.g., ReOH–Ir [21,50].

The ring opening reaction of glycidol was considered as an alternative method to selectively valorize glycerol. The behavior of glycidol on ReOH–Rh was found qualitatively different from that of tetrahydrofurfuryl alcohol, pointing toward a ring size effect. As the ReOH–Rh catalyst was unable to effectively catalyze glycidol ring opening, a very strong acid may be necessary to reach good selectivity. The experimental preference toward 1,2-PDO on bare metal catalysts is not reproduced by the studied ring opening mechanisms, suggesting the reaction instead proceeds through an initial hydrogenation step.

Heterogeneous acid catalysis is an important avenue for producing value-added chemicals from abundant feedstocks like glycerol, and in this study, some of the relevant mechanisms have been examined in detail. Several catalytically relevant phenomena arising from the interplay between acid, metal and reactant properties were highlighted, including competition between acid and metal catalysis, acid–metal bifunctionality and a ring-size effect on proton-assisted ring opening reactions. The deeper atomic-level understanding of these features helps guide future research and development efforts in the fields of acid catalysis and biomass valorization.

Data availability

The computational data is available in Etsin Fair Data Service. The link to the data is given in the Supplementary Data Section.

Declaration of Competing Interest

The authors declare that they have no known competing financial interests or personal relationships that could have appeared to influence the work reported in this paper.

Acknowledgements

GS and KH acknowledge the financial support from Tekes (2671/31/2013). GS would also like to thank SERB, DST-India (project code- ECRA/2016/001975, Date-03.01.2017) and Science and Technology Department, Odisha (project code-27562800512017/201296ST, Date-24.02.2018) for financial support at NIT Rourkela. The computational resources were provided by the Finnish Grid and Cloud Initiative as well as the CSC – IT Center for Science, Espoo, Finland (https://www.csc.fi/en)

Appendix A. Supplementary material

Supplementary data associated with this article can be found, in the online version, at https://doi.org/10.1016/j.jcat.2023.03.032. The structure files for adsorption and transition states are available at https://doi.org/10.23729/6b20d3c8-8416-4f90-9035-07f1d9c5b9e0.

References

[1] M. Pagliaro, R. Ciriminna, H. Kimura, M. Rossi, C. Della Pina, From glycerol to value-added products, Angew. Chem., Int. Ed. 46 (2007) 4434–4440.
[2] C.-H.C. Zhou, J.N. Beltramini, Y.-X. Fan, G.Q.M. Lu, Chemoselective catalytic conversion of glycerol as a biorenewable source to valuable commodity chemicals, Chem. Soc. Rev. 37 (2008) 527–549.
[3] J. ten Dam, U. Hanefeld, Renewable chemicals: Dehydroxylation of glycerol and polyols, ChemSusChem 4 (2011) 1017–1034.
[4] Y.-C. Lin, Catalytic valorization of glycerol to hydrogen and syngas, Int. J. Hydrogen Energy 38 (2013) 2678–2700.
[5] E.S. Vasiliadou, A.A. Lemonidou, Glycerol transformation to value added c3 diols: reaction mechanism, kinetic, and engineering aspects, Wiley Interdiscip. Rev. Energy Environ. 4 (2015) 486–520.
[6] K. Tomishige, Y. Nakagawa, M. Tamura, Selective hydrogenolysis and hydrogenation using metal catalysts directly modified with metal oxide species, Green Chem. 19 (2017) 2876–2924.
[7] L. Du, Y. Shao, J. Sun, G. Yin, C. Du, Y. Wang, Electrocatalytic valorisation of biomass derived chemicals, Catal. Sci. Technol. 8 (2018) 3216–3232.
[8] H. Liu, X. Ou, S. Zhou, D. Liu, Microbial 1,3-propanediol, its copolymerization with terephthalate, and applications, in: G.G.-Q. Chen (Ed.), Plastics from Bacteria: Natural Functions and Applications, Springer, Berlin Heidelberg, Berlin, Heidelberg, 2010, pp. 405–425, https://doi.org/10.1007/978-3-642-03287-5_16.
[9] L. Gong, Y. Lu, Y. Ding, R. Lin, J. Li, W. Dong, T. Wang, W. Chen, Selective hydrogenolysis of glycerol to 1,3-propanediol over a pt/wo_3/tio_2/sio_2 catalyst in aqueous media, Appl. Catal., A 390 (2010) 119–126.
[10] Y. Nakagawa, Y. Shinmi, S. Koso, K. Tomishige, Direct hydrogenolysis of glycerol into 1,3-propanediol over rhenium-modified iridium catalyst, J. Catal. 272 (2010) 191–194.
[11] M. Chia, Y.J. Pagán-Torres, D. Hibbitts, Q. Tan, H.N. Pham, A.K. Datye, M. Neurock, R.J. Davis, J.A. Dumesic, Selective hydrogenolysis of polyols and cyclic ethers over bifunctional surface sites on rhodium–rhenium catalysts, J. Am. Chem. Soc. 133 (2011) 12675–12689.
[12] E.S. Vasiliadou, A.A. Lemonidou, Parameters affecting the formation of 1,2-propanediol from glycerol over ru/sio_2 catalyst, Org. Process Res. Dev. 15 (2011) 925–931.
[13] S. Koso, Y. Nakagawa, K. Tomishige, Mechanism of the hydrogenolysis of ethers over silica-supported rhodium catalyst modified with rhenium oxide, J. Catal. 280 (2011) 221–229.
[14] K. Kongpatpanich, T. Nanok, B. Boekfa, M. Probst, J. Limtrakul, Structures and reaction mechanisms of glycerol dehydration over h-zsm-5 zeolite: a density functional theory study, Phys. Chem. Chem. Phys. 13 (2011) 6462–6470.
[15] D.D. Falcone, J.H. Hack, A.Y. Klyushin, A. Knop-Gericke, R. Schlögl, R.J. Davis, Evidence for the bifunctional nature of pt–re catalysts for selective glycerol hydrogenolysis, ACS Catal. 5 (2015) 5679–5695.
[16] M.A. Dasari, P.-P. Kiatsimkul, W.R. Sutterlin, G.J. Suppes, Low-pressure hydrogenolysis of glycerol to propylene glycol, Appl. Catal., A 281 (2005) 225–231.
[17] F. Auneau, C. Michel, F. Delbecq, C. Pinel, P. Sautet, Unravelling the mechanism of glycerol hydrogenolysis over rhodium catalyst through combined experimental–theoretical investigations, Chem. – Eur. J. 17 (2011) 14288–14299.
[18] D. Coll, F. Delbecq, Y. Aray, P. Sautet, Stability of intermediates in the glycerol hydrogenolysis on transition metal catalysts from first principles, Phys. Chem. Chem. Phys. 13 (2011) 1448–1456.
[19] B. Liu, J. Greeley, A density functional theory analysis of trends in glycerol decomposition on close-packed transition metal surfaces, Phys. Chem. Chem. Phys. 15 (2013) 6475–6485.
[20] Y. Shinmi, S. Koso, T. Kubota, Y. Nakagawa, K. Tomishige, Modification of rh/sio_2 catalyst for the hydrogenolysis of glycerol in water, Appl. Catal., B 94 (2010) 318–326.
[21] Y. Amada, Y. Shinmi, S. Koso, T. Kubota, Y. Nakagawa, K. Tomishige, Reaction mechanism of the glycerol hydrogenolysis to 1,3-propanediol over ir–reo_x/sio_2 catalyst, Appl. Catal., B 105 (2011) 117–127.
[22] M. Tamura, Y. Amada, S. Liu, Z. Yuan, Y. Nakagawa, K. Tomishige, Promoting effect of ru on ir-reo_x/sio_2 catalyst in hydrogenolysis of glycerol, J. Mol. Catal. A: Chem. 388–389 (2014) 177–187.
[23] L. Liu, T. Asano, Y. Nakagawa, M. Tamura, K. Okumura, K. Tomishige, Selective hydrogenolysis of glycerol to 1,3-propanediol over rhenium-oxide-modified iridium nanoparticles coating rutile titania support, ACS Catal. 9 (2019) 10913–10930.
[24] M.L. Gothe, K.L.C. Silva, A.L. Figueredo, J.L. Fiorio, J. Rozendo, B. Manduca, V. Simizu, R.S. Freire, M.A.S. Garcia, P. Vidinha, Rhenium – a tuneable player in tailored hydrogenation catalysis, Eur. J. Inorg. Chem. 2021 (2021) 4043–4065.
[25] C. Montassier, D. Giraud, J. Barbier, Polyol conversion by liquid phase heterogeneous catalysis over metals, in: M. Guisnet, J. Barrault, C. Bouchoule, D. Duprez, C. Montassier, G.Pérot (Eds.), Heterogeneous Catalysis and Fine Chemicals, volume 41 of Stud. Surf. Sci. Catal., Elsevier, 1988, pp. 165–170. URL: https://www.sciencedirect.com/science/article/pii/S0167299109608119. doi:10.1016/S0167-2991(09)60811-9.
[26] Y. Wang, J. Zhou, X. Guo, Catalytic hydrogenolysis of glycerol to propanediols: a review, RSC Adv. 5 (2015) 74611–74628.
[27] C. Michel, F. Auneau, F. Delbecq, P. Sautet, C–h versus o–h bond dissociation for alcohols on a rh(111) surface: A strong assistance from hydrogen bonded neighbors, ACS Catal. 1 (2011) 1430–1440.
[28] J. Zaffran, C. Michel, F. Delbecq, P. Sautet, Towards more accurate prediction of activation energies for polyalcohol dehydrogenation on transition metal catalysts in water, Catal. Sci. Technol. 6 (2016) 6615–6624.
[29] M. Valter, E.C.d. Santos, L.G.M. Pettersson, A. Hellman, Selectivity of the first two glycerol dehydrogenation steps determined using scaling relationships, ACS Catal. 11 (2021) 3487–3497.
[30] J.J. Mortensen, L.B. Hansen, K.W. Jacobsen, Real-space grid implementation of the projector augmented wave method, Phys. Rev. B 71 (2005) 035109.
[31] J. Enkovaara, C. Rostgaard, J.J. Mortensen, J. Chen, M. Dułak, L. Ferrighi, J. Gavnholt, C. Glinsvad, V. Haikola, H.A. Hansen, H.H. Kristoffersen, M. Kuisma, A.H. Larsen, L. Lehtovaara, M. Ljungberg, O. Lopez-Acevedo, P.G. Moses, J. Ojanen, T. Olsen, V. Petzold, N.A. Romero, J. Stausholm-Møller, M. Strange, G.A. Tritsaris, M. Vanin, M. Walter, B. Hammer, H. Häkkinen, G.K.H. Madsen, R.M. Nieminen, J.K. Nørskov, M. Puska, T.T. Rantala, J. Schiøtz, K.S. Thygesen, K.W. Jacobsen, Electronic structure calculations with GPAW: a real-space implementation of the projector augmented-wave method, J. Phys.: Condens. Matter 22 (2010) 253202.
[32] P.E. Blöchl, Projector augmented-wave method, Phys. Rev. B 50 (1994) 17953–17979.
[33] A.H. Larsen, J.J. Mortensen, J. Blomqvist, I.E. Castelli, R. Christensen, M. Dułak, J. Friis, M.N. Groves, B. Hammer, C. Hargus, E.D. Hermes, P.C. Jennings, P.B. Jensen, J. Kermode, J.R. Kitchin, E.L. Kolsbjerg, J. Kubal, K. Kaasbjerg, S. Lysgaard, J.B. Maronsson, T. Maxson, T. Olsen, L. Pastewka, A. Peterson, C. Rostgaard, J. Schiøtz, O. Schütt, M. Strange, K.S. Thygesen, T. Vegge, L. Vilhelmsen, M. Walter, Z. Zeng, K.W. Jacobsen, The atomic simulation environment—a python library for working with atoms, J. Phys.: Condens. Matter 29 (2017) 273002.
[34] J.P. Perdew, K. Burke, M. Ernzerhof, Generalized gradient approximation made simple, Phys. Rev. Lett. 77 (1996) 3865–3868.
[35] A. Tkatchenko, M. Scheffler, Accurate molecular van der waals interactions from ground-state electron density and free-atom reference data, Phys. Rev. Lett. 102 (2009) 073005.
[36] T. Gould, T. Bucko, C6 coefficients and dipole polarizabilities for all atoms and many ions in rows 1–6 of the periodic table, J. Chem. Theory Comput. 12 (2016) 3603–3613.
[37] G. Henkelman, B.P. Uberuaga, H. Jónsson, A climbing image nudged elastic band method for finding saddle points and minimum energy paths, J. Chem. Phys. 113 (2000) 9901–9904.
[38] S. Smidstrup, A. Pedersen, K. Stokbro, H. Jónsson, Improved initial guess for minimum energy path calculations, J. Chem. Phys. 140 (2014) 214106.
[39] E.L. Kolsbjerg, M.N. Groves, B. Hammer, An automated nudged elastic band method, J. Chem. Phys. 145 (2016) 094107.
[40] P. Tereshchuk, A.S. Chaves, J.L.F. Da Silva, Glycerol adsorption on platinum surfaces: A density functional theory investigation with van der waals corrections, J. Phys. Chem. C 118 (2014) 15251–15259.
[41] J. Chaminand, L. Djakovitch, P. Gallezot, P. Marion, C. Pinel, C. Rosier, Glycerol hydrogenolysis on heterogeneous catalysts, Green Chem. 6 (2004) 359–361.
[42] I. Furikado, T. Miyazawa, S. Koso, A. Shimao, K. Kunimori, K. Tomishige, Catalytic performance of rh/sio_2 in glycerol reaction under hydrogen, Green Chem. 9 (2007) 582–588.

[43] J.-H. Wang, C.S. Lee, M.C. Lin, Mechanism of ethanol reforming: Theoretical foundations, J. Phys. Chem. C 113 (2009) 6681–6688.
[44] M. Li, W. Guo, R. Jiang, L. Zhao, X. Lu, H. Zhu, D. Fu, H. Shan, Density functional study of ethanol decomposition on rh(111), J. Phys. Chem. C 114 (2010) 21493–21503.
[45] Y. Choi, P. Liu, Understanding of ethanol decomposition on rh(111) from density functional theory and kinetic monte carlo simulations, Catal. Today 165 (2011) 64–70.
[46] J.E. Sutton, D.G. Vlachos, Ethanol activation on closed-packed surfaces, Ind. Eng. Chem. Res. 54 (2015) 4213–4225.
[47] X.-K. Gu, B. Liu, J. Greeley, First-principles study of structure sensitivity of ethylene glycol conversion on platinum, ACS Catal. 5 (2015) 2623–2631.
[48] Y. Choi, P. Liu, Mechanism of ethanol synthesis from syngas on rh(111), J. Am. Chem. Soc. 131 (2009) 13054–13061.
[49] H. Li, G. Henkelman, Dehydrogenation selectivity of ethanol on close-packed transition metal surfaces: A computational study of monometallic, pd/au, and rh/au catalysts, J. Phys. Chem. C 121 (2017) 27504–27510.
[50] J.J. Varghese, L. Cao, C. Robertson, Y. Yang, L.F. Gladden, A.A. Lapkin, S.H. Mushrif, Synergistic contribution of the acidic metal oxide–metal couple and solvent environment in the selective hydrogenolysis of glycerol: A combined experimental and computational study using reox–ir as the catalyst, ACS Catal. 9 (2019) 485–503.
[51] R.T. Hannagan, G. Giannakakis, M. Flytzani-Stephanopoulos, E.C.H. Sykes, Single-atom alloy catalysis, Chem. Rev. 120 (2020) 12044–12088.
[52] D. Hibbitts, Q. Tan, M. Neurock, Acid strength and bifunctional catalytic behavior of alloys comprised of noble metals and oxophilic metal promoters, J. Catal. 315 (2014) 48–58.
[53] S. Koso, H. Watanabe, K. Okumura, Y. Nakagawa, K. Tomishige, Comparative study of rh–moo_x and rh–reo_x supported on sio_2 for the hydrogenolysis of ethers and polyols, Appl. Catal., B 111–112 (2012) 27–37.
[54] S. Koso, I. Furikado, A. Shimao, T. Miyazawa, K. Kunimori, K. Tomishige, Chemoselective hydrogenolysis of tetrahydrofurfuryl alcohol to 1,5-pentanediol, Chem. Commun. (2009) 2035–2037.
[55] K. Chen, S. Koso, T. Kubota, Y. Nakagawa, K. Tomishige, Chemoselective hydrogenolysis of tetrahydropyran-2-methanol to 1,6-hexanediol over rhenium-modified carbon-supported rhodium catalysts, ChemCatChem 2 (2010) 547–555.
[56] T. Buntara, S. Noel, P.H. Phua, I. Melián-Cabrera, J.G. de Vries, H.J. Heeres, Caprolactam from renewable resources: Catalytic conversion of 5-hydroxymethylfurfural into caprolactone, Angew. Chem., Int. Ed. 50 (2011) 7083–7087.
[57] Y. Zhou, F. Ouyang, Z.-B. Song, Z. Yang, D.-J. Tao, Facile one-pot synthesis of glycidol from glycerol and dimethyl carbonate catalyzed by tetraethylammonium amino acid ionic liquids, Catal. Commun. 66 (2015) 25–29.
[58] P. Prete, D. Cespi, F. Passarini, C. Capacchione, A. Proto, R. Cucciniello, Glycidol syntheses and valorizations: Boosting the glycerol biorefinery, Curr. Opin. Green Sustainable Chem. 35 (2022) 100624.
[59] F. Gebretsadik, J. Ruiz-Martinez, P. Salagre, Y. Cesteros, Glycidol hydrogenolysis on a cheap mesoporous acid saponite supported ni catalyst as alternative approach to 1,3-propanediol synthesis, Appl. Catal., A 538 (2017) 91–98.
[60] F.B. Gebretsadik, J. Llorca, P. Salagre, Y. Cesteros, Hydrogenolysis of glycidol as an alternative route to obtain 1,3-propanediol selectively using mo_x-modified nickel-copper catalysts supported on acid mesoporous saponite, ChemCatChem 9 (2017) 3670–3680.
[61] H. Sajiki, K. Hattori, K. Hirota, Pd/c(en)-catalyzed regioselective hydrogenolysis of terminal epoxides to secondary alcohols, Chem. Commun. (1999) 1041–1042.
[62] R. Cucciniello, C. Pironti, C. Capacchione, A. Proto, M. Di Serio, Efficient and selective conversion of glycidol to 1,2-propanediol over pd/c catalyst, Catal. Commun. 77 (2016) 98–102.
[63] Y. Sun, Z. Cai, X. Li, P. Chen, Z. Hou, Selective synthesis of 1,3-propanediol from glycidol over a carbon film encapsulated co catalyst, Catal. Sci. Technol. 9 (2019) 5022–5030.
[64] M. Mahapatra, W.T. Tysoe, Chemisorptive enantioselectivity of chiral epoxides on tartaric-acid modified pd(111): three-point bonding, Phys. Chem. Chem. Phys. 17 (2015) 5450–5458.
[65] J. Macht, R.T. Carr, E. Iglesia, Consequences of acid strength for isomerization and elimination catalysis on solid acids, J. Am. Chem. Soc. 131 (2009) 6554–6565.
[66] J. Guan, J. Li, Y. Yu, X. Mu, A. Chen, Dft studies of the selective c–o hydrogenolysis and ring-opening of biomass-derived tetrahydrofurfuryl alcohol over rh(111) surfaces, J. Phys. Chem. C 120 (2016) 19124–19134.
[67] S. Wang, V. Vorotnikov, D.G. Vlachos, Coverage-induced conformational effects on activity and selectivity: Hydrogenation and decarbonylation of furfural on pd(111), ACS Catal. 5 (2015) 104–112.